Solid-state optical properties of the methyl-exopyridine-anthracene rotaxane

Gadret, Gregory; Zamboni, Roberto; Schouwink, Peter; Mahrt, Rainer F.; Thies, Jens; Loontjens, Ton; Leigh, David A.

Published in:
Chemical Physics

DOI:
10.1016/S0301-0104(01)00272-5

Publication date:
2001

ELSEVIER

Chemical Physics 269 (2001) 381–388

Chemical Physics

www.elsevier.nl/locate/chemphys

Solid-state optical properties of the methyl-exopyridine–anthracene rotaxane

Gregory Gadret [a,b,*], Roberto Zamboni [a], Peter Schouwink [b], Rainer F. Mahrt [b], Jens Thies [c], Ton Loontjens [c], David A. Leigh [d]

[a] *Istituto di Spettroscopia Molecolare, Consiglio Nazionale delle Ricerche, via P. Gobetti 101, 40129 Bologna, Italy*
[b] *Max Planck Institut für Polymerforschung, Ackermannweg 10, 50128 Mainz, Germany*
[c] *DSM Research, 6160 MD Geleen, The Netherlands*
[d] *Centre for Supramolecular and Macromolecular Chemistry, University of Warwick, Coventry CV4 7AL, UK*

Received 24 October 2000

Abstract

Photophysical properties in the solid state of both, an anthracene grafted rotaxane and the corresponding thread are studied. The thread in liquid and solid states as well as the rotaxane in the liquid phase exhibit only the usual anthracene-like photoluminescence (PL) behaviour, while the rotaxane polycrystalline powder emits a broad structureless red-shifted band. The excitation spectrum of the rotaxane reveals the presence of low-lying states below the absorption feature of the anthracene, the one of the thread reproducing quite accurately the absorption spectrum. Site-selective PL measurements show that the broad emission of the rotaxane is a superposition of two contributions corresponding to energy levels which can be photoexcited directly within the low energy absorption tail. Time resolved PL measurements reveals immediately after excitation the characteristic features of the anthracene-like emission, indicating an energy transfer from the excited anthracene moiety to the structural defect states giving rise to the unusual radiative emission.

Keywords: Anthracene; Rotaxane; Solid-state; Optical spectroscopy

1. Introduction

Rotaxanes are mechanically interlocked hydrogen-bond assembled supramolecular organic systems having unique architectural and structural properties [1]. Schematically they consist of a macrocycle threaded by a ''linear'' molecular rod possessing bulky molecular stoppers at each end. The linear thread contains units where the macrocycle can be held by hydrogen bonding. Controlling the later will allow the macrocycle to move along the thread in a mechanically constrained way due to the stoppers.

New relevant optoelectronical and optomechanical properties have been demonstrated from this class of materials, particularly switching and gating in the liquid phase [2–4]. Recently, electrically induced refractive index variations due to the circumrotation of the macrocycle has been demonstrated in the liquid phase [5]. Moreover, the

* Corresponding author. Address: Max Planck Institut für Polymerforschung, Ackermannweg 10, 50128 Mainz, Germany. Tel.: +49-06131-379-493; fax: +49-06131-379-100.
E-mail address: gadret@mpip-mainz.mpg.de (G. Gadret).

0301-0104/01/$ - see front matter
PII: S0301-0104(01)00272-5

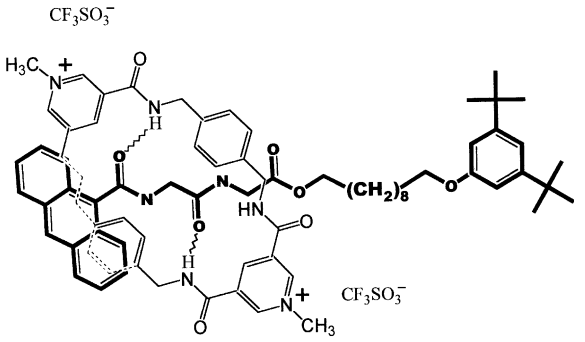

Fig. 1. Schematized chemical structure of epar–me. The thread is drawn using bold bonds, hydrogen bonds are drawn as "wavy" bonds.

unique architecture of this class of compounds supplies new physico-chemical configurations which could allow to control intramolecular electron and energy transfer.

Here we report on spectroscopic investigation of photophysical properties of the methyl-exopyridine–anthracene rotaxane (epar–me). The chemical structure of epar–me is shown in Fig. 1, where the 10-[3,5-di(terbutyl)phenoxy]decyl-2-({2-[(9-anthrylcarbonyl)amino]acetyl}amino)acetate (thread) is drawn in bold. The macrocycle, including two methyl-pyridinium groups (electron acceptors A), is threaded by a linear peptide group/alkyl chain molecule limited by two stoppers, a bis-terbutylbenzylic ring at one end and a nine-position grafted anthracene moiety (electron donor D) at the other end. In the solid state, the macrocycle is hydrogen bonded to the peptide station, which is the base configuration resulting from the templating synthesis process [1]. Consequently, although the A and D groups stand in very close proximity, the only possible intramolecular through-bond interactions between them involve the hydrogen bonding pattern located between the peptide station of the thread and the amine groups included in the macrocycle.

Photoluminescence (PL) properties of anthracene derivatives have been studied extensively for a long time. These works have been led on a wide range of supermolecules, mostly in the liquid phase and in crystalline structures, and the reasons for the emission of a broad red-shifted unstructured PL spectrum have been explained in various ways, depending on the molecular configuration and on the environment of the optically active entities. Intermolecular interactions like sandwich dimers [6] and excimers [7,8], through-space and through-bond electron transfer [9] and interactions with the solvent [10] can give rise to a dual fluorescence effect where the observed additional spectral feature is a broad unstructured red-shifted band. In particular, charge separation has been evidenced in D–A compounds, where both the active groups are included in the same supermolecule and separated by a spacer. In the liquid phase, this spacer may consist of solvent [11], hydrogen bridging groups [12] or covalent bonds between D and A moieties [13–15].

We have investigated the optical behaviour of both the thread and epar–me polycrystalline powders. To characterize these compounds, we have performed room temperature absorption along with photoluminescence excitation measurements (PLE), steady-state and time resolved PL as well as site-selective photoluminescence (SSPL) at both, room and low temperature.

2. Experiment

Most of the results were obtained using polycrystalline powders. Films investigated for absorption measurements were obtained by spin coating from solutions in spectroscopic grade dichloromethane (CH_2Cl_2), ethylacetate (EthOAc) and dimethylformamide (DMF). As substrate we used fused silica or sapphire plates for absorption and PL measurements. For PLE measurements we used fused silica or silicon plates, on which polycrystalline powders were gently ground in such a way to lower the sample absorbance, thus avoiding any skin effect which could strongly alter the measurements.

Absorption measurements were performed at 293 K on a Jasco V500 UV–VIS spectrophotometer. Steady-state PL spectra were obtained using the 365.5 nm line of an extended argon laser (Coherent innova 70) as excitation and liquid helium temperature was reached using a Janis SVT bath cryostat. We used a Hamamatsu PMA-11 optical multichannel analyzer to detect the signal.

The source used for PLE was a 300 W Xenon lamp (Osram XBO 300). The white light was coupled into a computer controlled Spectrapro 275 monochromator (1200 g/mm holographic grating, slits width set for a ±4 nm spectral resolution) via an UV grade fused silica optical fiber bundle. In order to normalize accurately the PLE spectra, detection of the excitation intensity and measured signal were simultaneously achieved using two RCA R928 side-on photomultipliers and two PAR5209 lock-in detections synchronized by a light chopper located at the output of the monochromator. Because the spectral sensitivity of the photomultipliers is nearly flat in the investigated range, we did not perform any further correction. The detection energy was selected using a Jobin-Yvon H20 monochromator, equipped with a pair of 1 mm width slits allowing a spectral resolution of ±5 nm. Low temperature measurements were obtained by means of an Oxford cold-finger cryostat. Low temperature SSPL measurements were achieved using a 20 ns pulse duration excimer pumped dye laser (LambdaPhysics) as a tunable source. Samples were mounted into an Oxford cold-finger cryostat, and a Spex 270M optical multichannel analyzer was used for the detection. A MIRA 900 Kerr lens mode-locked Ti:sapphire laser (Coherent) producing 120 fs duration pulses at a repetition rate of 80 MHz followed by a frequency doubling BBO crystal were used to get the near UV excitation beam required for PL decay-time measurements. The emitted light was dispersed by a monochromator (grating 50 grooves/mm) and monitored by a streak camera system allowing a time resolution of 3 ps (Hamamatsu C4792-95). Low temperature measurements were achieved using an Oxford static flow cryostat.

3. Results

Room temperature absorption spectra of spin coated films of both thread and epar–me are depicted in Fig. 2(a) and (b) respectively. The 22 000–32 000 cm^{-1} spectral range is, for both compounds, driven by the anthracene-like absorption, the methylpyridinium groups absorbing at higher energy.

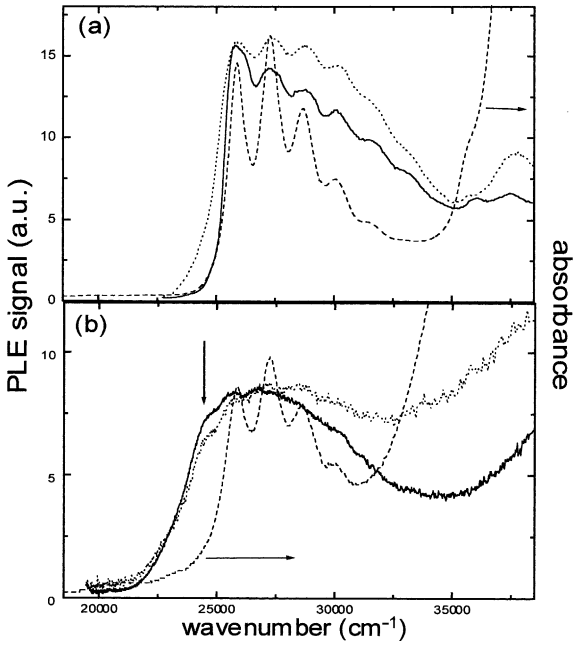

Fig. 2. (a) Excitation spectrum of the thread polycrystalline powder at 293 K (···) and 16 K (—) and room temperature absorption spectrum of a spin coated film from a solution of dichloromethane (- - -). For PLE measurements, the detection energy was set to 21 740 cm^{-1} at both the temperatures; (b) excitation spectrum of epar–me polycrystalline powder at 293 K (···) and 16 K (—) and room temperature absorption spectrum of a spin coated film from a solution of ethylacetate (- - -). For PLE measurements, the detection energy was set to 18 180 cm^{-1} at 293 K and 18 690 cm^{-1} at 16 K.

Thus, they exhibit a clear vibronic progression involving the 1412 cm^{-1} breathing mode of the anthracene-like moiety, the 0–0 transition being located at 25 770 cm^{-1}. Another assigned active Raman mode of the anthracene derivatives, located at 400 cm^{-1}, is partly responsible for the broadening of each main vibronic line of the spectrum. A careful inspection of the low energy tails shows that the absorption spectrum of epar–me is slightly broader than the one of the thread. Those spectra have been measured on spin coated films from CH_2Cl_2 and EthOAc solutions for both the compounds, showing no discrepancies.

Thread room and low temperature PLE spectra are depicted in Fig. 2(a) together with the absorption spectrum described above. These excitation spectra reproduce precisely the absorption

features, the discrepancy at high energy being not significant since the molecular and consequently the sample absorbance increase strongly in this range. At 16 K, the PLE spectrum is sharpened by thermal depopulation, revealing the 400 cm^{-1} vibronic mode of the anthracene, confirming the good spectral resolution of the measurements. Room and low temperature PLE spectra of epar–me are less structured than in the case of the thread, nevertheless they resemble the absorption spectrum, as depicted in Fig. 2(b). However, a low lying feature centered at 24 390 cm^{-1} is pointed out, which is totally absent in the PLE spectrum of the thread powder. When the sample is cooled down to 16 K, this additional feature remains located at the same energy, but its relative contribution to the overall integrated spectrum is slightly increased. We observe at high energy a non-relevant discrepancy which is due, as for the thread, to the increasing molecular absorbance. The PLE spectra of both thread and epar–me are essentially independent on the detection wavelength.

Thread steady-state PL spectra measured at room and liquid helium temperatures are depicted in Fig. 3. At both temperatures we observe an anthracene-like behaviour, where the emission spectrum resembles the mirror image of the absorption. Due to thermal depopulation, each line

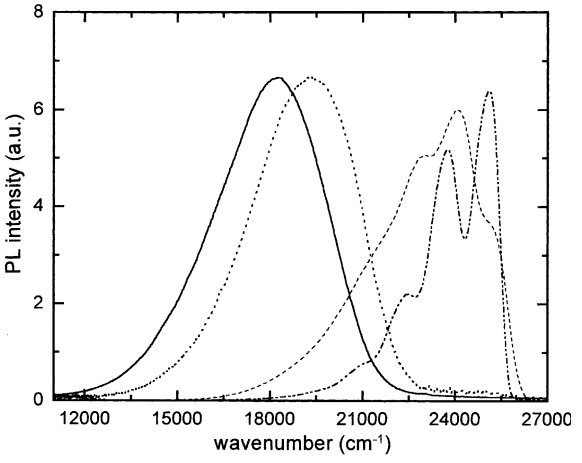

Fig. 3. PL spectra of polycrystalline powders: thread at 293 K (- - -) and 4.2 K (-·-·-); epar–me at 293 K (—) and 4.2 K (···). The excitation energy is 27 360 cm^{-1}.

of the vibronic progression is sharpened at low temperature, together with the absorption spectrum as seen in PLE measurements. Thus, the anthracene-like Franck–Condon distribution is completely resolved, and the vanishing reabsorption effect allows to clearly point out the 0–0 origin of the PL at 25 100 cm^{-1}. The PL spectrum of epar–me (Fig. 3) consists of an unstructured broad red-shifted band (FWHM 4300 cm^{-1}), the characteristic anthracene-like vibronic progression being completely absent. The maximum emission energy, located at 18 180 cm^{-1} at 293 K, is substantially blue-shifted (1235 cm^{-1}) when the sample is cooled down to 4.2 K, this process being totally reversible. At this point, it is worth to notice that both epar–me and thread room and low temperature solutions in CH_2Cl_2 (weakly polar) and DMF (strongly polar) exhibit the classical anthracene-like emission spectrum. The molar concentration used for these measurements (not showed there) was 2×10^{-5}.

We performed low temperature SSPL measurements in order to determine whether the PL behaviour of epar–me is affected by the excitation energy (Fig. 4). The spectrally narrow excitation laser line allows to photoexcite selectively the low lying levels. Here, a superposition of two contributions, located at 18 430 cm^{-1} (band A) and 17 400 cm^{-1} (band B) respectively, are pointed out in the overall PL spectrum. The amplitude of the band A decreases when the excitation energy is tuned across the absorption profile to lower energies (from 25 316 to 21 277 cm^{-1}). The B band remains fairly unchanged in shape, however it is slightly red-shifted (450 cm^{-1}).

Additionally, we have performed decay time measurements at low temperature in order to refine the relaxation mechanism of both the compounds. The early time fluorescence spectrum of the thread exhibits the characteristic features of the anthracene-like vibronic progression, following a purely monoexponential decay law ($\tau =$ 20–30 ns) in the whole corresponding spectral range. The early time PL behaviour of epar–me is depicted in Fig. 5(a). During the first 10 ps after photoexcitation, a vibronic progression matching the one of the anthracene is observed. It is however substantially red-shifted ($\approx$1340 cm^{-1})

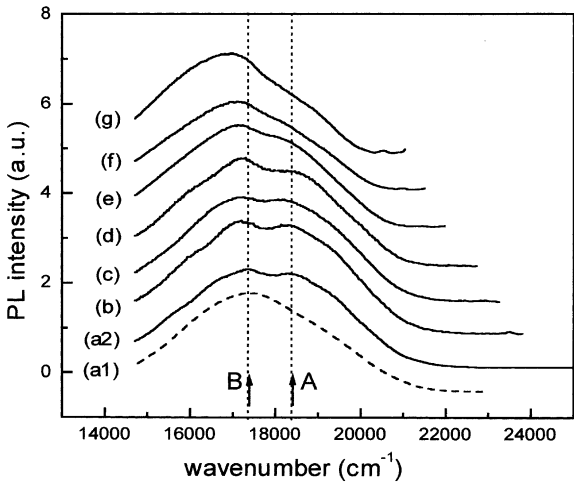

Fig. 4. SSPL measurements of epar–me. Measurement temperatures are 293 K for the (a1) dashed curve and 4.2 K for the others. Excitation energies are: (a1) 25 316 cm^{-1}, (a2) 25 316 cm^{-1}, (b) 24 096 cm^{-1}, (c) 23 529 cm^{-1}, (d) 22 988 cm^{-1}, (e) 22 222 cm^{-1}, (f) 21 739 cm^{-1}, (g) 21 277 cm^{-1}. All the curves are normalized and vertically shifted for clarity. The two arrows indicate the maximum emission energy (excitation at 25 316 cm^{-1}) of the two contributions, labelled A and B. Vertical dotted lines are a guide for the eyes.

with respect to the location of the 0–0 anthracene-like PL band in the thread (see Fig. 3). This contribution relaxes on a fast time scale and vanishes after 80 ps, giving rise to the broad red-shifted emission band dominating the steady-state emission spectrum. At high energy, where both the contributions are superimposed, the decay process is biexponential (Fig. 5(c)), becoming monoexponential at lower energy (Fig. 5(b)). The decay time τ_0 corresponding to the early time anthracene-like relaxation takes values in the range 5–11 ps, whereas the τ_1 parameter, characterizing the low energy decay process, appears highly dependent on energy (Fig. 6).

4. Discussion

The SSPL measurements, performed at 4.2 K, show that the emitting levels responsible for the broad red-shifted emission of the epar–me polycrystalline powder can be photoexcited directly within the low energy tail of the absorption band.

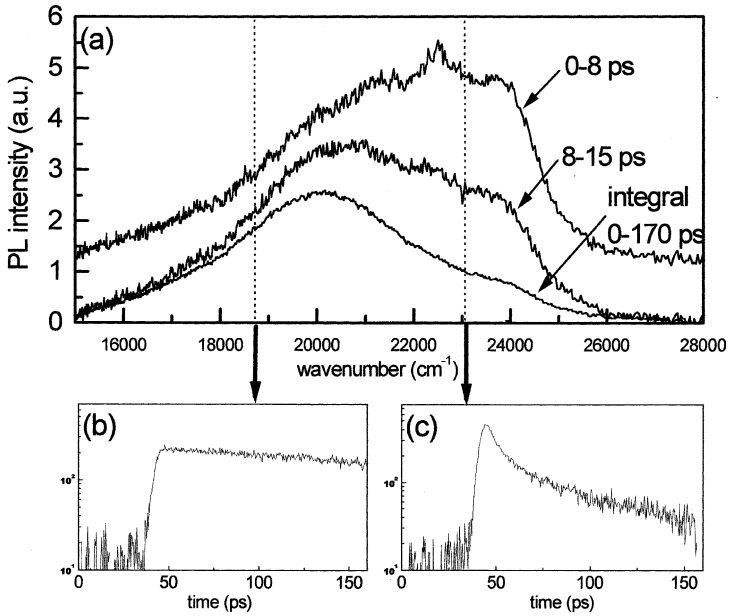

Fig. 5. (a) Time resolved fluorescence of epar–me (for the sake of clarity, the curve 0–8 ps has been vertically translated); transients detected at (b) 18 700 cm^{-1} and (c) 23 040 cm^{-1}, displayed in logarithmic scale. The corresponding decay times are (b) $\tau_1 = 306$ ps, (c) $\tau_0 = 8$ ps and $\tau_1 = 73$ ps.

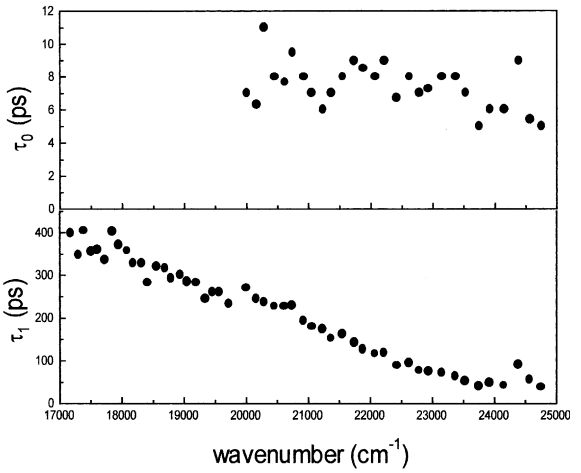

Fig. 6. Energy dependence of epar–me decay times.

Moreover, these data allow to point out the structure of the emission band, which appears to be build up from two contributions, centered at 18 430 cm^{-1} (band A) and 17 400 cm^{-1} (band B). The A peak nearly disappears when the excitation energy is tuned down to 21 277 cm^{-1}, suggesting that it originates from levels located higher in energy. At the latter excitation energy, the B emission is still clearly visible. In both, room and low temperature epar–me PLE spectra, ground state levels are pointed out within the tail of absorption with a maximum peaked at 24 390 cm^{-1} (Fig. 2). This is confirmed by the broadness of the absorption spectrum in the same range. The low energy tail of this distribution of states is located at 20 000–21 000 cm^{-1}, as seen in PLE, matching reasonably the excitation range in which the A PL band almost vanishes, as demonstrated by SSPL. We consequently infer that the low lying levels detected in PLE give rise to the A PL band, whereas the levels responsible for the B emission are located are lower energy and could not be revealed by PLE measurements. The red-shift of the B band observed in SSPL measurements after tuning of the excitation wavelength could be related to the inhomogeneous broadening of the corresponding emitting levels. The related concentration is too low to be seen in the PLE spectrum, which consequently does not depend on the detection energy. As well, the room temperature absorption spectrum could not allow to work out these lowest lying ground state levels, because this technique is poorly sensitive to the very low concentrated absorbing states.

Time resolved PL measurements performed on epar–me show that the anthracene-like excited state relaxes via both radiative and non-radiative channels. In fact, the anthracene-like vibronic progression is visible at early time after photoexcitation (Fig. 5(a)). In the corresponding energy range (22 000–25 000 cm^{-1}), the decay process is biexponential (Fig. 5(c)), with a fast decay parameter τ_0 lying within the range 5–11 ps. The second decay parameter τ_1 is energy dependent (Fig. 6), taking values from 50 ps at 25 000 cm^{-1} up to 400 ps at the low energy edge of the PL emission (17 000 cm^{-1}). The very short decay time of the anthracene-like contribution appears to be due to an efficient energy transfer to the lower lying states. The nature of these states could be physical aggregates and/or structural/morphological defects related to the flexibility of the epar–me rotaxane allowing to many favourable structural conformations. The associated density of states is broad (see Fig. 2(b)) and a filling process of the lowest lying levels occurs, explaining the energy dependence of the τ_1 parameter. After non-radiative relaxation, a purely monoexponential decay process is observed at low energy (Fig. 5(b)).

The anthracene-like features visible in the early time epar–me PL spectrum are substantially red-shifted (1430 cm^{-1}) with respect to the anthracene-like PL spectrum measured on the thread powder. This value is in good agreement with the vibronic progression of the anthracene-like vibronic structure (1412 cm^{-1}), suggesting reabsorption of the 0–0 luminescence transition. However, such an effect can be reasonably ruled out, since it does not occur in the thread powder at the same temperature (Fig. 3). In fact, the ground state behaviours of both compounds appear quite similar, as seen in absorption measurements (Fig. 2). In the case of the epar–me rotaxane, the observed red-shift suggests an increased solid-state effect in which the macrocycle may be involved.

A particular behaviour of the epar–me steady-state PL spectrum concerns the structured steady-state PL observed in SSPL, where excitation energy

is tuned from 25 316 cm^{-1} down to 21 277 cm^{-1}. In particular, the room temperature SSPL spectrum corresponding to an excitation at 25 316 cm^{-1} (dashed curve (a1) in Fig. 4) resembles the low temperature one recorded after excitation at 21 277 cm^{-1} (curve (g) in Fig. 4). This suggests that the relaxation path depends on the excitation conditions, namely the spectral position of the laser line, and the sample temperature as well. We have showed above that the epar–me emission originates from two different distributions of structural defects, labeled A and B, respectively centered at 24 390 cm^{-1} and lying below 21 277 cm^{-1}. Then, a reasonable explanations of the epar–me PL behaviour is supplied by the different concentrations of trapping sites associated to the A and B bands. In fact, the energetic interval between the 0–0 anthracene-like absorption band and the center of the A absorption band is about 1000 cm^{-1}, corresponding to a temperature of about 300 K. At room temperature, photoexcitation within the 0–0 anthracene-like origin leads to a PL spectrum dominated by the B emission band (curve (a1) in Fig. 4). This suggests a detrapping effect occurring at room temperature between A states and anthracene-like levels, followed by a non-radiative decay to the B states (see process depicted in Fig. 7(a)). In fact, the low concentration of B sites within the material does not allow a direct energy transfer from A to B states. At low temperature (curve (a2)), the detrapping effect is no longer thermally allowed and both A and B states are populated simultaneously by non-radiative decay from the anthracene-like absorption region. Consequently, both emissions from A and B levels are observed (Fig. 7(b)). As a confirmation, the curves (a1) and (g) (Fig. 4) appear similar, although they have been recorded respectively at 293 K (excitation at 25 316 cm^{-1}) and 4.2 K (excitation at 21 277 cm^{-1}). The B emission is in fact dominating for both the curves, but the corresponding relaxation processes are quite different, since, for the (a1) data, B levels are populated after detrapping, whereas they are directly filled by non-radiative relaxation for the (g) curve. These two relaxation processes are depicted respectively in Fig. 7(a) and (c).

However, the structure observed in SSPL is no longer visible in the PL spectrum measured after excitation with the 27 360 cm^{-1} line of an argon laser (Fig. 3). A similar structureless spectral behaviour is showed by the time-resolved integrated spectrum emitted after excitation with the 27 360 cm^{-1} centered broad line of the Ti:sapphire source (Fig. 5). In both cases, the same spectral shape and temperature dependent behaviour are pointed out. Further investigations are in progress in order to understand this complicated behaviour, as well as the blue-shift (1000–1200 cm^{-1}) of epar–me emission observed from room to low temperature, which could be related to the temperature dependent multi-trapping effect.

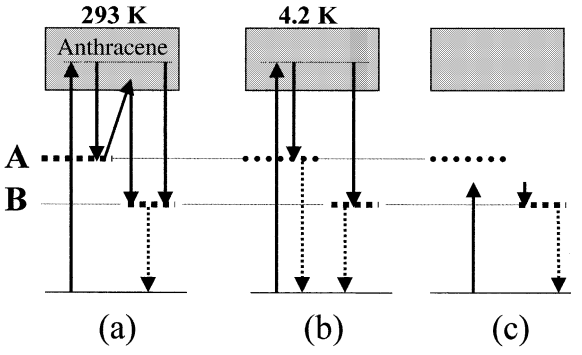

Fig. 7. Schematic diagram of the photophysical processes taking place in epar–me versus temperature and excitation energy. Radiative decays are indicated in dotted lines.

5. Conclusion

Using room and low temperature steady-state and time resolved spectroscopy, we have worked out the origin of PL from the methyl-exopyridine–anthracene rotaxane polycrystalline powder.

The optical behaviour of the epar–me rotaxane appears to be dominated by low lying state structural defects emission after fast energy transfer from the excited anthracene-like moiety. Thus, we point out the existence of two distributions of structural defects, related to different concentration within the compound.

Because of the ground state origin of the emitting levels, D–A interactions involving the anthracene-like moiety and the methyl-pyridinium groups belonging to the macrocycle, as well as intermolecular anthracene excimers could not be evidenced.

The nature of the structural defects responsible for energy trapping and emission is an open question, since the crystalline structure of the material is not available. However, recent studies on oligothiophenes allowed to point out the importance of structure and morphology, and particularly the control of polycrystalline texture and grain size and boundaries, on determining the dynamics and the spectral behaviour of radiative emission [16,17]. Indeed, the epar–me solid-state structure is expected to be relevantly influenced by its unusual supramolecular structure and as a matter of fact, the early time anthracene-like emission appears to be red-shifted with respect to the thread PL spectrum.

Acknowledgements

We acknowledge financial support from the European Community Training and Mobility of Researchers program no. FMRX CT97-0097, Development of Rotaxane-based Unconventional Materials (DRUM), and from the Max-Planck Gesellschaft.

References

[1] D.A. Leigh, A. Murphy, J.P. Smart, A.M.Z. Slawin, Angew. Chem. Int. Ed. 36 (7) (1997) 728.
[2] A. Credi, V. Balzani, S.J. Langford, J.F. Stoddart, J. Am. Chem. Soc. 119 (1997) 2679.
[3] V. Balzani, M. Gomez-Lopez, J.F. Stoddart, Acc. Chem. Res. 31 (1998) 405.
[4] E. Ishow, A. Credi, V. Balzani, F. Spadola, L. Mandolini, Chem. Eur. J. 5 (3) (1999) 984.
[5] V. Bermudez, N. Capron, T. Gase, F.G. Gatti, F. Kajzar, D.A. Leigh, F. Zerbetto, S. Zhang, Nature 406 (2000) 608.
[6] J. Ferguson, A.W.-H. Mau, J.M. Morris, Aust. J. Chem. 26 (1973) 91.
[7] M.D. Cohen, Z. Ludmer, V. Yakhot, Phys. Stat. Sol. (b) 67 (1975) 51.
[8] M. Pope, C.E. Swenberg, Electronic Processes in Organic Crystals and Polymers, Oxford University Press, Oxford, 1999.
[9] D. Gosztola, B. Wang, M.R. Wasielewski, J. Photochem. Photobiol. A: Chem. 102 (1996) 71.
[10] T.C. Werner, J. Rodgers, J. Photochem. 32 (1986) 59.
[11] J.R. Miller, J.V. Beitz, R.K. Huddleston, J. Am. Chem. Soc. 106 (1984) 5057.
[12] J.L. Sessler, B. Wang, A. Harriman, J. Am. Chem. Soc. 117 (1995) 704.
[13] T. Hirsch, H. Port, H.C. Wolf, B. Miehlich, F. Effenberger, J. Phys. Chem. B 101 (1997) 4525.
[14] D. Gust, T.A. Moore, A.L. Moore, Acc. Chem. Res. 26 (1993) 198.
[15] H. Kurreck, M. Huber, Angew. Chem. Int. Ed. Engl. 34 (1995) 849.
[16] R.N. Marks, M. Muccini, E. Lunedei, R. Michel, M. Murgia, R. Zamboni, C. Taliani, G. Horowitz, F. Garnier, M. Hopmeier, M. Oestreich, R.F. Mahrt, Chem. Phys. 227 (1998) 49.
[17] M. Hopmeier, W. Gebauer, M. Oestreich, M. Sokolowski, E. Umbach, R.F. Mahrt, Chem. Phys. Lett. 314 (1999) 9.